

# Towards automatic protein backbone assignment using proton-detected 4D solid-state NMR data

ShengQi Xiang · Veniamin Chevelkov ·  
Stefan Becker · Adam Lange

Received: 23 July 2014 / Accepted: 28 August 2014 / Published online: 6 September 2014  
© Springer Science+Business Media Dordrecht 2014

**Abstract** We introduce an efficient approach for sequential protein backbone assignment based on two complementary proton-detected 4D solid-state NMR experiments that correlate  $H_i^N/N_i$  with  $CA_i/CO_i$  or  $CA_{i-1}/CO_{i-1}$ . The resulting 4D spectra exhibit excellent sensitivity and resolution and are amenable to (semi-)automatic assignment approaches. This strategy allows to obtain sequential connections with high confidence as problems related to peak overlap and multiple assignment possibilities are avoided. Non-uniform sampling schemes were implemented to allow for the acquisition of 4D spectra within a few days. Rather moderate hardware requirements enable the successful demonstration of the method on deuterated type III secretion needles using a 600 MHz spectrometer at a spinning rate of 25 kHz.

**Keywords** Proton-detection · Sparse sampling · MAS solid-state NMR · (Semi-)automatic backbone assignment · Type III secretion needles

**Electronic supplementary material** The online version of this article (doi:10.1007/s10858-014-9859-6) contains supplementary material, which is available to authorized users.

S. Xiang · V. Chevelkov · S. Becker · A. Lange (✉)  
Department of NMR-based Structural Biology, Max Planck  
Institute for Biophysical Chemistry, Am Fassberg 11,  
37077 Göttingen, Germany  
e-mail: adla@nmr.mpibpc.mpg.de

V. Chevelkov · A. Lange  
Leibniz-Institut für Molekulare Pharmakologie, Robert-Rössle-  
Str. 10, 13125 Berlin, Germany

A. Lange  
Institut für Biologie, Humboldt-Universität zu Berlin, Berlin,  
Germany

## Introduction

Solid-state NMR (ssNMR) is a unique technique to gain atomic-level insights into structure and dynamics of insoluble biomolecules such as microcrystalline proteins (Igumenova et al. 2004; Knight et al. 2012), amyloid fibrils (Tycko 2011), supramolecular assemblies (Han et al. 2010; Loquet et al. 2012) and membrane proteins in liposomes (Chen et al. 2014; Hu et al. 2010; Lange et al. 2006; Wang 2013). Compared to traditional ssNMR experiments in which normally signals from  $^{13}C$  or  $^{15}N$  are detected, proton detection (Ishii et al. 2001; Reif and Griffin 2003) can further extend the scope of ssNMR by enhancing spectral sensitivity because of the high gyromagnetic ratio of  $^1H$  and by improving resolution via the additional observable nucleus.

Backbone assignment, associating NMR signals to the backbone nuclei of a certain residue, is the first and essential step of every NMR study. For proton-detected experiments, several different backbone assignment strategies were developed depending on the protonation level. At ultra-fast spin rates (>40 kHz) and high external magnetic fields, fully protonated samples or perdeuterated samples with 100 % reprotonation can be utilized, which enables straightforward dipolar and scalar-based transfer pathways that correlate  $HN_i$  and  $N_i$  to carbon nuclei of residue  $i$  or  $i - 1$ , such as CA and CO, and even CB (Knight et al. 2011, 2012; Zhou et al. 2012). In contrast, partial reprotonation (ca 10–20 %) is required at moderate spinning rates and low external magnetic fields in order to obtain well resolved  $^1H$  spectra (Chevelkov et al. 2006; Linser 2012; Linser et al. 2008) for which a dipolar-based “out and back” magnetization transfer pathway was shown to yield superior sensitivity (Chevelkov et al. 2014; Linser 2012; Linser et al. 2008).

While higher dimensional NMR spectra offer better resolution and more information (Huber et al. 2011; Linser et al. 2011; Trent Franks et al. 2010; Wylie et al. 2014), they also exponentially increase the measurement time if a uniform sampling scheme is employed. Non-uniform sampling (NUS) methods provide a convenient way to circumvent the time barrier of high-dimensional NMR experiments (Jaravine et al. 2006). NUS schemes have been widely applied in solution NMR studies (Coggins et al. 2010; Hyberts et al. 2012; Orekhov et al. 2003). More recently, the usefulness of NUS in ssNMR has also been explored and validated (Huber et al. 2011; Jones and Opella 2006; Lin and Opella 2013; Linser 2014; Suiter et al. 2014; Sun et al. 2012; Trent Franks et al. 2010).

Taking advantage of proton detection and non-linear sampling, we designed a method to facilitate (semi-)automatic backbone assignment, which is based on two complementary proton-detected 4D magic-angle spinning (MAS) experiments. Currently, automatic backbone assignment is still not straightforward in ssNMR applications but promising first examples have been presented (Barbet-Massin 2014; Hu et al. 2011; Nielsen et al. 2014; Schmidt et al. 2013). The 4D correlations obtained from the two introduced experiments are ideal input information for automatic backbone assignment software such as MARS (Jung and Zweckstetter 2004). Here, we present a successful application of our 4D approach to an insoluble, non-crystalline protein assembly, the *Salmonella typhimurium* type III secretion system (T3SS) needle (Cornelis and WolfWatz 1997). The 80-residue subunit PrgI was uniformly  $^{13}\text{C}/^{15}\text{N}$  labeled and perdeuterated with 20 % re-protonation on exchangeable sites (Chevelkov et al. 2014) (Fig. S1).

## Materials and methods

### Sample preparation

Expression, purification and polymerization of perdeuterated  $^{15}\text{N}$ - and  $^{13}\text{C}$ -labeled PrgI protein was carried out as previously described (Chevelkov et al. 2014; Loquet et al. 2012). The sample was re-protonated in a buffer containing 20 %  $\text{H}_2\text{O}$  and 80 %  $\text{D}_2\text{O}$ . Approximately 3.5 mg of sample was packed into a 2.5 mm rotor.

### Solid-state NMR experiments

The experiments were carried out at a MAS rate of 25 kHz on a 14.1 T wide-bore spectrometer (Bruker Biospin, Germany), equipped with a 2.5 mm triple-resonance ( $^1\text{H}$ , X, Y) MAS probe. All chemical shifts were referenced to the signal of internal DSS. The sample temperature was kept at

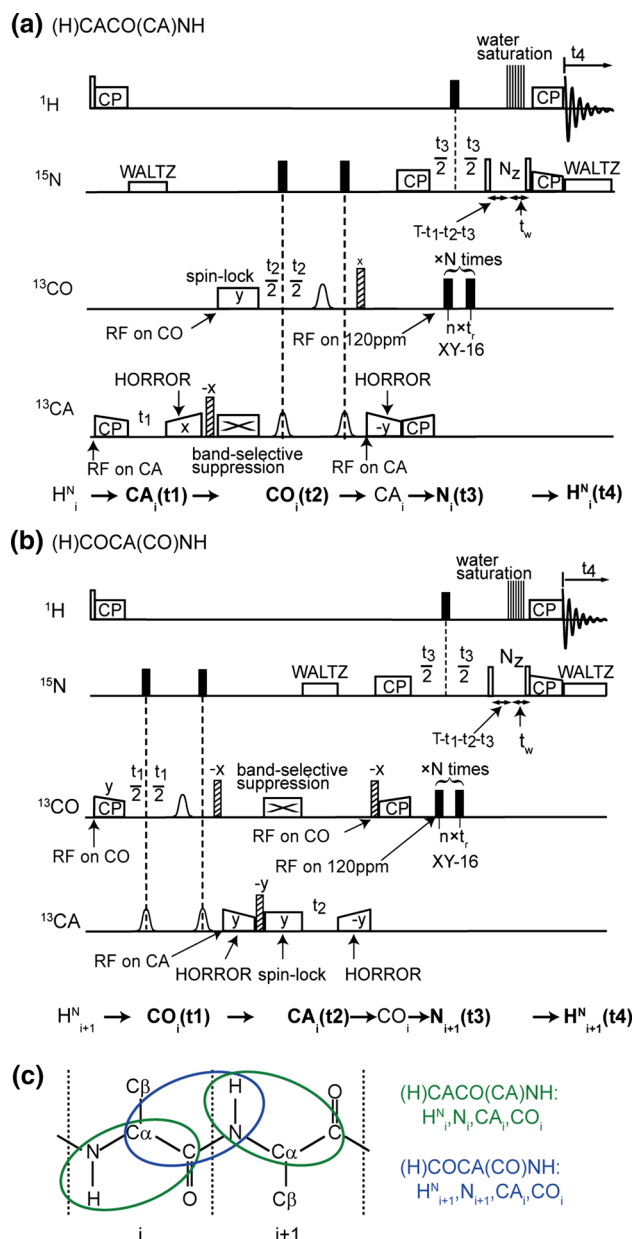


**Fig. 1** **a** (H)CACO(CA)NH pulse sequence to obtain intra-residual  $\text{HN}_i$ ,  $\text{N}_i$ ,  $\text{CA}_i$  and  $\text{CO}_i$  correlations. **b** (H)COCA(CO)NH pulse sequence to obtain inter-residual  $\text{HN}_{i+1}$ ,  $\text{N}_{i+1}$ ,  $\text{CA}_i$  and  $\text{CO}_i$  correlations. *Open, filled and striped bars* represent  $90^\circ$ ,  $180^\circ$  and trim pulses, respectively. *Bell shapes* indicate selective  $180^\circ$  pulses on CO and CA (Geen and Freeman 1991). **c** Schematic representation of the inter-spin correlations provided by the two experiments

284 K, which was measured by the position of the water proton resonance. The 2D (H)NH experiment was implemented as before (Chevelkov et al. 2014) (spectrum shown in Fig. S1). The maximum acquisition times were 65.8 ms for N and 40 ms for  $\text{H}^{\text{N}}$ .

The two pulse schemes are based on our previously described proton-detected 3D correlation experiments, and employ similar “out and back” transfer pathways

(Chevelkov et al. 2014). The (H)CACO(CA)NH pulse program provides intra-residue correlations of  $\text{HN}_i$ ,  $\text{N}_i$ ,  $\text{CA}_i$  and  $\text{CO}_i$  (Fig. 1a). The initial magnetization on  $\text{HN}_i$  is transferred to  $\text{CA}_i$  by cross polarization and then further distributed to  $\text{CO}_i$  employing HORROR (Nielsen et al. 1994). The remaining magnetization on CA is removed by a  $^{13}\text{C}$  spin-lock applied on the CO band, matching the rotary resonance condition on CA as described previously (Chevelkov et al. 2014). Subsequently, the magnetization is transferred back to  $\text{CA}_i$  using HORROR, then to  $\text{N}_i$  by CA–N SPECIFIC-CP (Baldus et al. 1998) and finally back to  $\text{HN}_i$  for detection. At times where the transverse magnetization is on  $\text{CO}_i$ ,  $\text{CA}_i$  and  $\text{N}_i$ , respectively, chemical shift evolution periods are inserted. During the  $\text{CO}_i$  evolution period, a  $180^\circ$  selective pulse on CA is applied to refocus CO–CA J couplings and a high-power  $180^\circ$  pulse on N to remove N–CO J couplings, whereas only waltz-16 (Shaka et al. 1983) is used for N–CA decoupling during the  $\text{CA}_i$  evolution period. During N evolution, N–CA and N–CO J couplings are removed by a train of  $180^\circ$  hard pulses with a XY-16 phase scheme (Gullion et al. 1990) applied in the middle of CO and CA bands.  $\text{H}^{\text{N}}$  is decoupled from N by a single  $180^\circ$  hard pulse in the middle of the N evolution period. Waltz-16 (Shaka et al. 1983) is applied on N during proton detection. The water signal is saturated by a proton pulse sequence while N magnetization is stored along the +z direction before transfer back to protons (Zhou and Rienstra 2008) (Experimental details can be found in the supplementary material).

The same approach with minor modifications can be used for the complementary (H)COCA(CO)NH experiment illustrated in Fig. 1b, which correlates  $\text{HN}_{i+1}$ ,  $\text{N}_{i+1}$ ,  $\text{CA}_i$  and  $\text{CO}_i$  (see also supplementary material).

To carry out these two 4D experiments with good sensitivity and resolution in a reasonable time frame, we adopted a NUS scheme that covered only 20 % of the full sampling space (NUS details can be found in the supplementary material). In this way, the experimental time of a single spectrum could be reduced from 27.5 to 5.5 days. Sparsely sampled datasets were then further processed by means of the mddNMR software (Orekhov et al. 2003).

## Results and discussion

In the first experiment, (H)CACO(CA)NH, four backbone atoms within the same residue,  $\text{HN}_i$ ,  $\text{N}_i$ ,  $\text{CA}_i$  and  $\text{CO}_i$  are correlated (pulse scheme shown in Fig. 1a). In the second complementary experiment, (H)COCA(CO)NH, the inter-residue correlations between  $\text{HN}_{i+1}$  and  $\text{N}_{i+1}$  with  $\text{CA}_i$  and  $\text{CO}_i$  are established (Fig. 1b). The  $\text{H}^{\text{N}}$  and N atom pairs are used as “anchor points” the same way as in routine solution NMR backbone assignment strategies. The

connectivity between neighbouring anchor points is then obtained by matching chemical shifts of both CA and CO atoms. This approach efficiently reduces assignment ambiguities because the peaks are very well-separated in 4D space and two chemical shifts are simultaneously used to establish sequential connections.

The overall transfer efficiencies found were the same as in the previously reported 3D correlation experiments (Chevelkov et al. 2014). The first FID of the (H)COCA(CO)NH spectrum exhibits  $\sim 8\%$  intensity compared to the signal in a (H)NH 1D spectrum. Almost all residues give rise to signals except a few: the first four residues, N22, L23, K50 and S62. These residues were also weak or not visible in 2D and 3D correlation spectra as described in our previous study (Chevelkov et al. 2014).

The assignment strategy is illustrated in Fig. 2a by a sequential walk along the backbone of PrgI from residue K69 to D72. In the  $\text{H}^{\text{N}}$ –N 2D planes of the two 4D spectra defined by CA and CO chemical shifts of residue K69, each plane contains a single peak. The peak with chemical shifts  $\text{H}^{\text{N}}69$ , N69, CA69 and CO69, labelled as  $\text{H}^{\text{N}}69\text{N69}(\text{CA69CO69})$  (the two dimensions defining the 2D plane position in the 4D spectrum are indicated in brackets), is from the (H)CACO(CA)NH spectrum that reveals the intra-residue correlation (peak depicted in green). The other peak, labeled correspondingly as  $\text{H}^{\text{N}}70\text{N70}(\text{CA69CO69})$ , is from the (H)COCA(CO)NH spectrum yielding the inter-residue correlation (shown in blue).

From the peak  $\text{H}^{\text{N}}70\text{N70}(\text{CA69CO69})$ , the chemical shifts of  $\text{H}^{\text{N}}70$  and N70 can be obtained. After navigating to the CA–CO plane defined by the  $\text{H}^{\text{N}}70$  and N70 chemical shifts, again two peaks are observed in the two planes. The peak from the (H)COCA(CO)NH spectrum corresponds to the same correlation as the peak  $\text{H}^{\text{N}}70\text{N70}(\text{CA69CO69})$  discussed above, but is now labelled as  $\text{H}^{\text{N}}70\text{N70}(\text{CA70CO70})$ . The other peak is  $\text{H}^{\text{N}}70\text{N70}(\text{CA70CO70})$  from the (H)CACO(CA)NH spectrum. The chemical shift values of CA70 and CO70 are obtained from this peak and we can then proceed to the H–N 2D planes defined by CA70 and CO70 of both 4D spectra. Here, besides the known peak  $\text{H}^{\text{N}}70\text{N70}(\text{CA70CO70})$  from the (H)CACO(CA)NH spectrum, there is another peak from the (H)COCA(CO)NH spectrum.

This peak is  $\text{H}^{\text{N}}71\text{N71}(\text{CA70CO70})$  which provides the  $\text{H}^{\text{N}}$  and N chemical shifts of residue I71. The same process can be repeated and the sequential connectivity established.

To illustrate the high sensitivity and resolution of the recorded spectra, traces of the  $\text{H}^{\text{N}}70\text{N70CA70CO70}$  and  $\text{H}^{\text{N}}70\text{N70CA69CO69}$  peaks along all four dimensions are shown in Fig. 2b. The line width of CA is larger than of CO because CA–CO, CA–CB and CA– $^2\text{H}$  scalar couplings are not decoupled. The 2D  $\text{H}^{\text{N}}$ –N planes from the two 4D spectra defined by the CA69 and CO69 chemical shifts

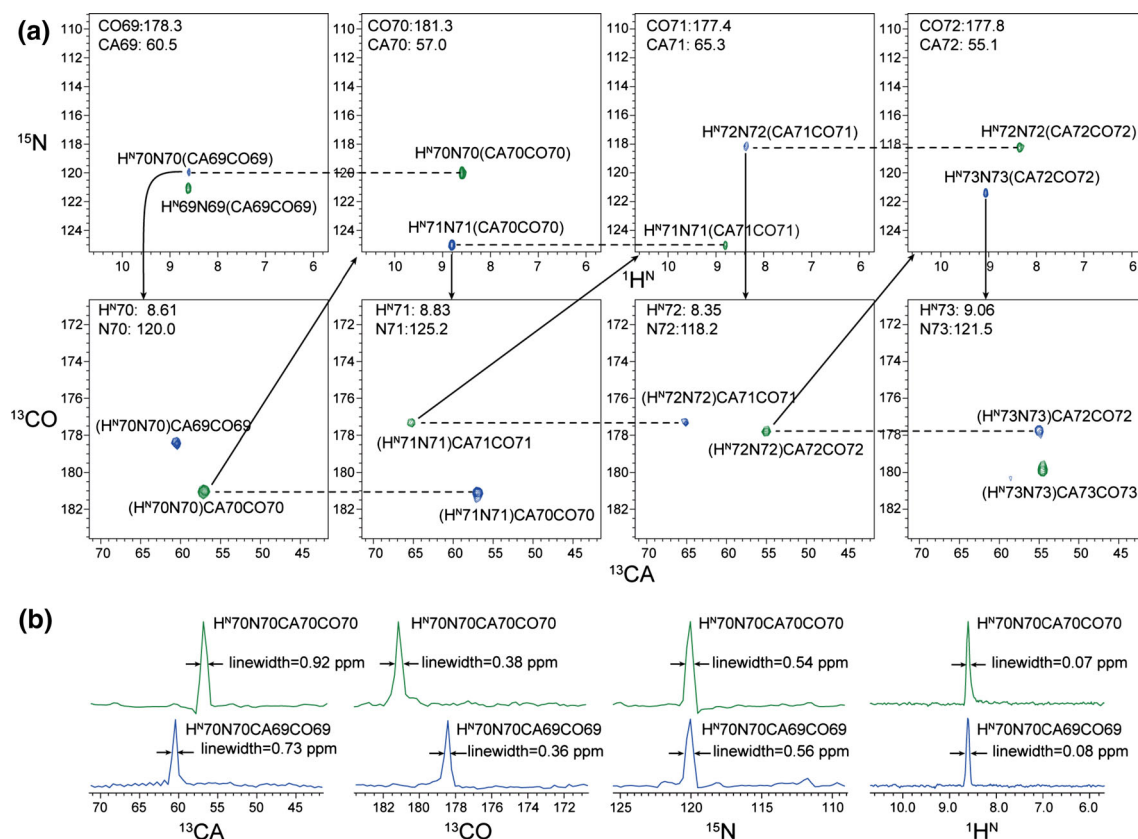


**Fig. 2** **a** 2D planes of 4D spectra are shown to illustrate the assignment procedure. The chemical shifts of the other two dimensions are shown in the *upper-left corner* of each 2D plane. Peaks from the (H)COCA(CO)NH spectrum are shown in *blue* and peaks from the (H)CACO(CA)NH spectrum in *green*. The peaks are labelled in such a way that the two dimensions that define the 2D plane position

in the 4D spectra are indicated in *brackets*. *Arrows* correspond to the working flow during the walk along the backbone. *Dashed lines* connect pairs of peaks with the same chemical shifts in both dimensions of the planes. **b** Traces of  $\text{H}^{\text{N}}70\text{N}70\text{CA}70\text{CO}70$  (*green*) and  $\text{H}^{\text{N}}70\text{N}70\text{CA}69\text{CO}69$  (*blue*) along all four dimensions. Line-widths (FWHM) are indicated

overlay very well with the corresponding correlations in the 2D (H)NH correlation spectrum (Fig. S2), which demonstrates the high resolution and accuracy of peak positions in the 4D spectra.

The input for (semi-)automatic backbone assignment software is prepared as follows: For every  $\text{H}^{\text{N}}\text{-N}$  peak in the 2D (H)NH spectrum (Chevelkov et al. 2014) (see Fig. S1), one obtains  $\text{CO}_i$  and  $\text{CA}_i$  shifts from the (H)CACO(-CA)NH spectrum, and  $\text{CO}_{i-1}$  and  $\text{CA}_{i-1}$  shifts from the (H)COCA(CO)NH spectrum. This results in a spin system table containing entries of six chemical shift values:  $\text{HN}_i$ ,  $\text{N}_i$ ,  $\text{CA}_i$ ,  $\text{CO}_i$ ,  $\text{CA}_{i-1}$  and  $\text{CO}_{i-1}$ , which is suitable input for (semi-)automatic backbone assignment software. Then the correlations between  $\text{H}^{\text{N}}\text{-N}$  pairs are established by matching CA and CO chemical shifts.

One merit of our approach is that the connection between  $\text{H}^{\text{N}}\text{-N}$  anchor points is always based on two chemical shifts: CA and CO. This significantly reduces the ambiguity of sequential connections. In case of small proteins such as PrgI, this method achieves sequential

connectivity without any ambiguity. With 0.5 ppm for CA and 0.2 ppm for CO as tolerances of chemical shift mismatch, the sequential connectivity is unique throughout the whole sequence. These tolerance values fit well to the peak line-widths observed in the corresponding dimensions (Fig. 2b). The mismatch values of sequential connectivity are shown in Fig. 3a, b, c and d (as generated by the software MARS). In contrast, if only either CA or CO chemical shift are employed, numerous possible connections remain within the same tolerance (Fig. 3e, f).

In this study, we used MARS (Jung and Zweckstetter 2004) successfully to obtain sequential connections between visible signals in the 2D (H)NH spectrum. This procedure constitutes a semi-automatic approach. In principle, the generated data could be readily combined with side chain information and mapped onto the primary sequence to obtain a complete assignment table.

Our approach is not limited to the two experimental schemes described above as long as the same correlation

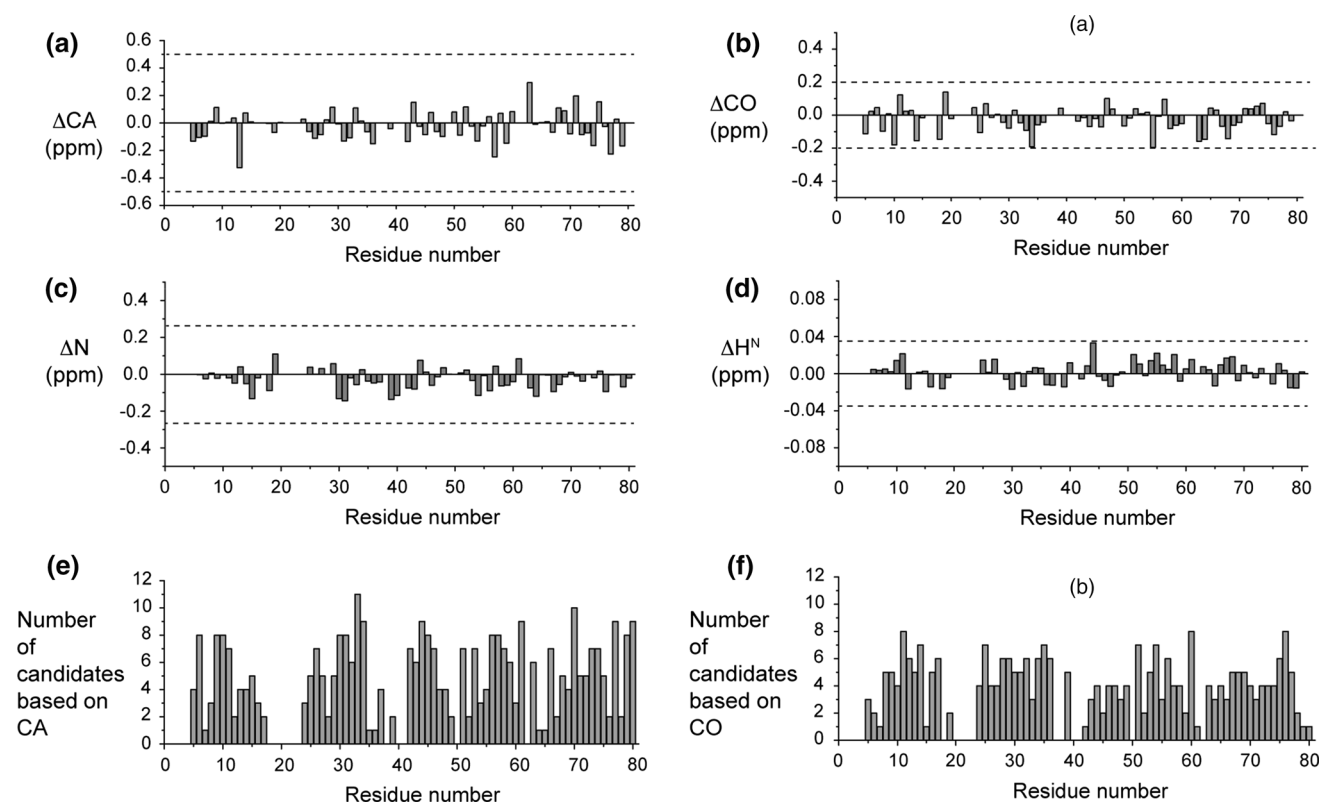


**Fig. 3** **a** The mismatch of CA chemical shifts in sequential connections. **b** The mismatch of CO chemical shifts in sequential connections. *Dashed lines* indicate the cutoff values,  $\pm 0.5$  ppm for CA and  $\pm 0.2$  ppm for CO. **c** The mismatch of N chemical shifts in sequential connections. **d** The mismatch of  $H^N$  chemical shifts in sequential connections. *Dashed lines* indicate half of the line widths

(FWHM),  $\pm 0.25$  ppm for N and  $\pm 0.035$  ppm for  $H^N$ . **e** The number of possible sequential connections within the cut-off of CA for each residue as a function of sequence. **f** The corresponding number based on CO. All panels were generated using the MARS software (Jung and Zweckstetter 2004)

information is obtained from alternative experiments. For example, in the ultra-fast spinning regime (MAS rates  $>40$  kHz) and at high external magnetic fields, perdeuterated samples with 100 % reprotonation on exchangeable sites or even fully protonated samples may be used (Knight et al. 2011; Zhou et al. 2012) instead. In this case, direct transfer pathways may be superior (Knight et al. 2011; Zhou et al. 2012) to “out and back” transfer pathways as employed here.

## Conclusion

In summary, we have introduced an efficient semi-automatic backbone assignment approach based on two complementary proton-detected 4D experiments recorded with a NUS scheme. This method was successfully applied to a highly deuterated PrgI needle sample and implemented using relatively modest hardware. Provided that similar data quality could be obtained for supramolecular assemblies with larger subunits sizes than PrgI—possibly by performing the experiments at higher magnetic fields and

spin rates -, the described method should be of general use in solid-state NMR investigations of complex and large systems.

**Acknowledgments** We thank Karin Giller and Brigitta Angerstein for expert technical assistance. This work was supported by the Max Planck Society, the Leibniz-Institut für Molekulare Pharmakologie and the DFG (Emmy Noether Fellowship to A.L.). A.L. and S.X. acknowledge funding from the CRC803 (DFG).

## References

- Baldus M, Petkova AT, Herzfeld J, Griffin RG (1998) Cross polarization in the tilted frame: assignment and spectral simplification in heteronuclear spin systems. *Mol Phys* 95:1197–1207
- Barbet-Massin E (2014) Rapid proton-detected NMR assignment for proteins with fast magic angle spinning. *J Am Chem Soc* 136(35):12489–12497
- Chen YK, Zhang ZF, Tang XQ, Li JP, Glaubitz C, Yang J (2014) Conformation and topology of diacylglycerol kinase in *E. coli* membranes revealed by solid-state NMR spectroscopy. *Angew Chem Int Ed* 53:5624–5628
- Chevelkov V, Rehbein K, Diehl A, Reif B (2006) Ultrahigh resolution in proton solid-state NMR spectroscopy at high levels of deuteration. *Angew Chem Int Ed* 45:3878–3881

- Chevelkov V, Habenstein B, Loquet A, Giller K, Becker S, Lange A (2014) Proton-detected MAS NMR experiments based on dipolar transfers for backbone assignment of highly deuterated proteins. *J Magn Reson* 242:180–188
- Coggins BE, Venters RA, Zhou P (2010) Radial sampling for fast NMR: concepts and practices over three decades. *Prog Nucl Magn Reson Spectrosc* 57:381–419
- Cornelis GR, WolfWatz H (1997) The Yersinia Yop virulon: a bacterial system for subverting eukaryotic cells. *Mol Microbiol* 23:861–867
- Geen H, Freeman R (1991) Band-selective radiofrequency pulses. *J Magn Reson* 93:93–141
- Gullion T, Baker DB, Conradi MS (1990) New, compensated carrucell sequences. *J Magn Reson* 89:479–484
- Han Y, Ahn J, Concel J, Byeon IJL, Gronenborn AM, Yang J, Polenova T (2010) Solid-state NMR studies of HIV-1 capsid protein assemblies. *J Am Chem Soc* 132:1976–1987
- Hu FH, Luo WB, Hong M (2010) Mechanisms of proton conduction and gating in influenza M2 proton channels from solid-state NMR. *Science* 330:505–508
- Hu KN, Qiang W, Tycko R (2011) A general Monte Carlo/simulated annealing algorithm for resonance assignment in NMR of uniformly labeled biopolymers. *J Biomol NMR* 50:267–276
- Huber M, Hiller S, Schanda P, Ernst M, Boeckmann A, Verel R, Meier BH (2011) A proton-detected 4D solid-state NMR experiment for protein structure determination. *ChemPhysChem* 12:915–918
- Hyberts SG, Milbradt AG, Wagner AB, Arthanari H, Wagner G (2012) Application of iterative soft thresholding for fast reconstruction of NMR data non-uniformly sampled with multidimensional poisson gap scheduling. *J Biomol NMR* 52:315–327
- Igumenova TI, Wand AJ, McDermott AE (2004) Assignment of the backbone resonances for microcrystalline ubiquitin. *J Am Chem Soc* 126:5323–5331
- Ishii Y, Yesinowski JP, Tycko R (2001) Sensitivity enhancement in solid-state  $^{13}\text{C}$  NMR of synthetic polymers and biopolymers by  $^1\text{H}$  NMR detection with high-speed magic angle spinning. *J Am Chem Soc* 123:2921–2922
- Jaravine V, Ibraghimov I, Orekhov VY (2006) Removal of a time barrier for high-resolution multidimensional NMR spectroscopy. *Nat Methods* 3:605–607
- Jones DH, Opella SJ (2006) Application of maximum entropy reconstruction to PISEMA spectra. *J Magn Reson* 179:105–113
- Jung Y-S, Zweckstetter M (2004) Mars—robust automatic backbone assignment of proteins. *J Biomol NMR* 30:11–23
- Knight MJ et al (2011) Fast resonance assignment and fold determination of human superoxide dismutase by high-resolution proton-detected solid-state mas nmr spectroscopy. *Angew Chem Int Ed Engl* 50:11697–11701
- Knight MJ et al (2012) Structure and backbone dynamics of a microcrystalline metalloprotein by solid-state NMR. *Proc Natl Acad Sci USA* 109:11095–11100
- Lange A, Giller K, Hornig S, Martin-Eauclaire MF, Pongs O, Becker S, Baldus M (2006) Toxin-induced conformational changes in a potassium channel revealed by solid-state NMR. *Nature* 440:959–962
- Lin EC, Opella SJ (2013) Sampling scheme and compressed sensing applied to solid-state NMR spectroscopy. *J Magn Reson* 237:40–48
- Linser R (2012) Backbone assignment of perdeuterated proteins using long-range H/C-dipolar transfers. *J Biomol NMR* 52:151–158
- Linser R (2014) Solid-state NMR structure determination from diagonal-compensated proton–proton restraints. *J Am Chem Soc* 136(31):11002–11010
- Linser R, Fink U, Reif B (2008) Proton-detected scalar coupling based assignment strategies in MAS solid-state NMR spectroscopy applied to perdeuterated proteins. *J Magn Reson* 193:89–93
- Linser R, Bardiaux B, Higman V, Fink U, Reif B (2011) Structure calculation from unambiguous long-range amide and Methyl H-1-H-1 distance restraints for a microcrystalline protein with MAS solid-state NMR spectroscopy. *J Am Chem Soc* 133:5905–5912
- Loquet A et al (2012) Atomic model of the type III secretion system needle. *Nature* 486:276–279
- Nielsen NC, Bildsoe H, Jakobsen HJ, Levitt MH (1994) Double-quantum homonuclear rotary resonance: Efficient dipolar recovery in magic-angle spinning nuclear magnetic resonance. *J Chem Phys* 101:1805–1812
- Nielsen J, Kulminkskaya N, Bjerring M, Nielsen N (2014) Automated robust and accurate assignment of protein resonances for solid state NMR. *J Biomol NMR* 59:119–134
- Orekhov VY, Ibraghimov I, Billeter M (2003) Optimizing resolution in multidimensional NMR by three-way decomposition. *J Biomol NMR* 27:165–173
- Reif B, Griffin RG (2003)  $^1\text{H}$  detected  $^1\text{H},^{15}\text{N}$  correlation spectroscopy in rotating solids. *J Magn Reson* 160:78–83
- Schmidt E et al (2013) Automated solid-state NMR resonance assignment of protein microcrystals and amyloids. *J Biomol NMR* 56:243–254
- Shaka AJ, Keeler J, Frenkiel T, Freeman R (1983) An improved Sequence for broad-band decoupling—WALTZ-16. *J Magn Reson* 52:335–338
- Suiter C et al (2014) Sensitivity gains, linearity, and spectral reproducibility in nonuniformly sampled multidimensional MAS NMR spectra of high dynamic range. *J Biomol NMR* 59:57–73
- Sun SJ, Yan S, Guo CM, Li MY, Hoch JC, Williams JC, Polenova T (2012) A time-saving strategy for MAS NMR spectroscopy by combining nonuniform sampling and paramagnetic relaxation assisted condensed data collection. *J Phys Chem B* 116:13585–13596
- Trent Franks W, Atreya H, Szyperski T, Rienstra C (2010) GFT projection NMR spectroscopy for proteins in the solid state. *J Biomol NMR* 48:213–223
- Tycko R (2011) Solid-state NMR studies of amyloid fibril structure. *Annu Rev Phys Chem* 62:279–299
- Wang S (2013) Solid-state NMR spectroscopy structure determination of a lipid-embedded heptahelical membrane protein. *Nat Methods* 10:1007–1012
- Wylie BJ, Bhate MP, McDermott AE (2014) Transmembrane allosteric coupling of the gates in a potassium channel. *Proc Natl Acad Sci USA* 111:185–190
- Zhou DH, Rienstra CM (2008) High-performance solvent suppression for proton detected solid-state NMR. *J Magn Reson* 192:167–172
- Zhou D et al (2012) Solid-state NMR analysis of membrane proteins and protein aggregates by proton detected spectroscopy. *J Biomol NMR* 54:291–305